NASA TECHNICAL NOTE

NASA TN D-4604
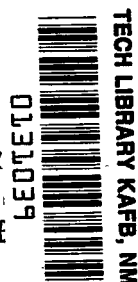
GENERAL OPERATING CHARACTERISTICS OF A BACK-STREAMING DIRECT-CURRENT PLASMA GENERATOR

by Roman Krawec

Lewis Research Center
Cleveland, Ohio

NATIONAL AERONAUTICS AND SPACE ADMINISTRATION • WASHINGTON, D. C. • JUNE 1968

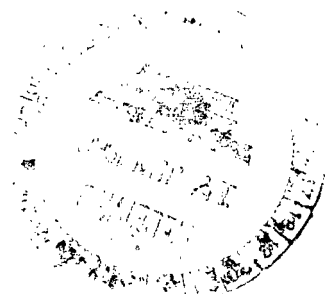NASA TN D-4604

GENERAL OPERATING CHARACTERISTICS OF A BACK-STREAMING

DIRECT-CURRENT PLASMA GENERATOR

By Roman Krawec

Lewis Research Center
Cleveland, Ohio

NATIONAL AERONAUTICS AND SPACE ADMINISTRATION

GENERAL OPERATING CHARACTERISTICS OF A BACK-STREAMING

DIRECT-CURRENT PLASMA GENERATOR

by Roman Krawec

Lewis Research Center

SUMMARY

Experimental studies were performed on a plasma generator consisting of a filament and a hollow, gas-fed anode which were immersed in an axial magnetic field. The hydrogen plasma formed between the filament and anode was allowed to diffuse past the filament, through a transition section, and into a low-pressure test section.

The plasma within the test section was characterized by having two groups of electrons which differed in temperature and had a peak density greater than 2×10^{12} centimeter^{-3}. The no-plasma background pressure within the test chamber was an order of magnitude less than the peak electron density. Evidence was found indicating that thermal dissociation of the hydrogen molecule occurred within the hollow anode.

INTRODUCTION

The present study was undertaken as part of a continuing effort to develop a more suitable magnetically confined plasma source for the Lewis Research Center ion cyclotron resonance experiment (ICRA 2, refs. 1 and 2). Previously reported means of generating a hydrogen plasma (ref. 3) used with this experiment were capable of meeting the criteria of ion density and plasma diameter; the percent ionization, however, was much lower than desired.

It was thus decided to depart from the previous approach, wherein the plasma was formed throughout the length of the experiment. Instead, the plasma was formed within a small region external to the main test section and guided into the test chamber by means of an axial magnetic field. The neutral gas pressure in the region of plasma formation was large compared to the pressure within the test chamber. This arrangement was expected to give efficient ionization within the source while at the same time permitting a low neutral background within the test section.

EXPERIMENTAL APPARATUS

Magnet and Vacuum Chamber

A schematic diagram of the experimental apparatus and the magnetic field configuration is given in figure 1. The vacuum system consisted of a source section and a test section, fabricated from commercially available 10-centimeter-inside-diameter glass pipe and connected together with a 5.1-centimeter-outside-diameter glass transition piece.
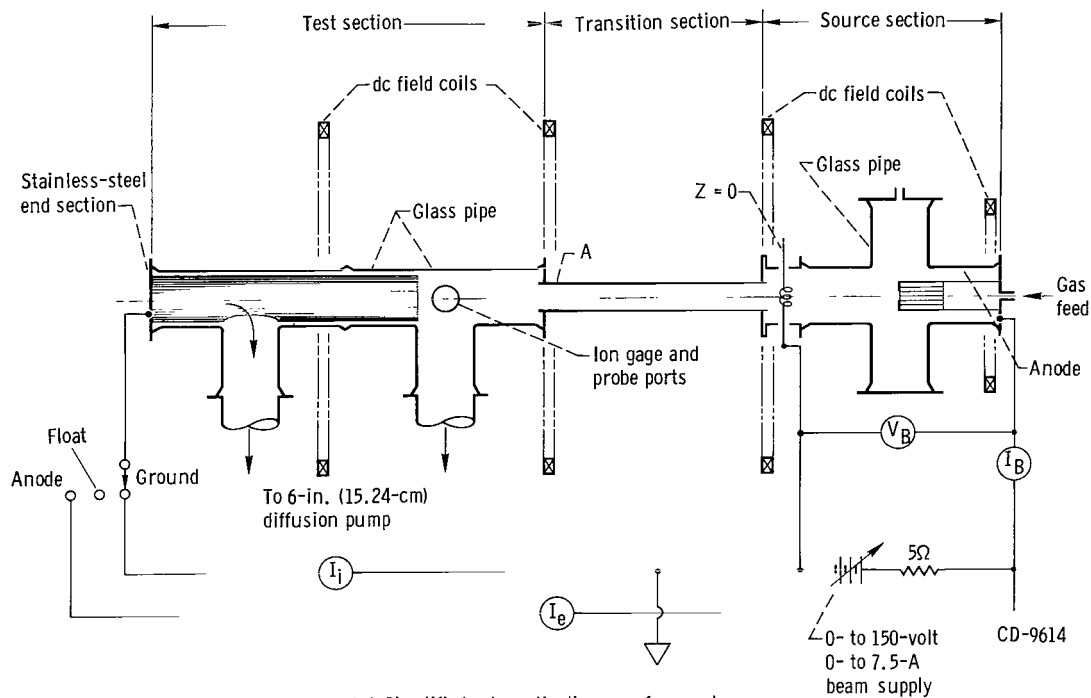
(a) Simplified schematic diagram of apparatus.

Figure 1. - Apparatus and magnetic field configuration.

A part of the test section consisted of a cylindrical metal can with one end closed and the other open to receive the plasma and was designed so that the plasma source could be tested under three modes of operation. The first mode of operation consisted of attaching the metal cylinder to ground, thereby simulating the injection of plasma into a grounded metal vacuum chamber. The cylindrical can could also be left unconnected to simulate operation into a floating test section or into free space; or it could be attached to the anode, simulating the case where the filament is operated at a negative potential with the test section and anode being at ground potential.
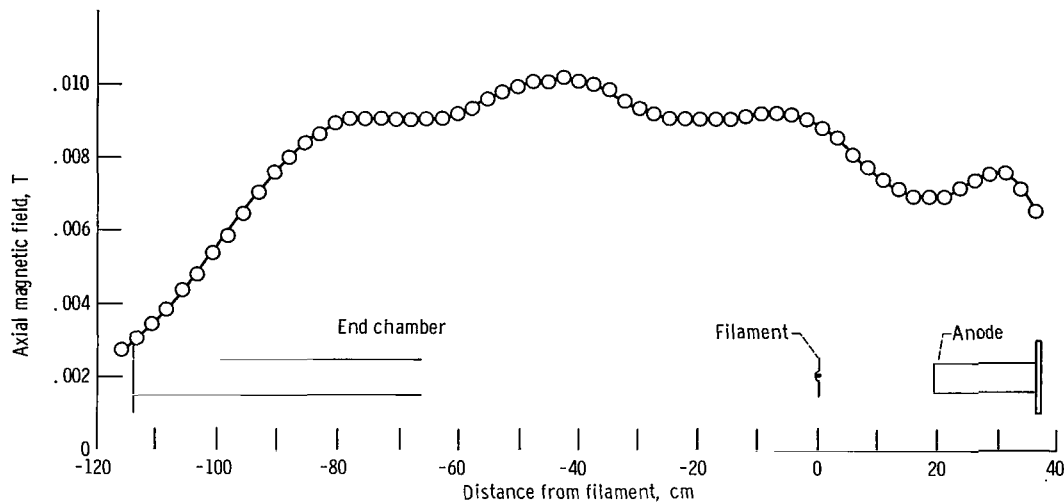
(b) Axial variation of magnetic field.

Figure 1. - Concluded.

A commercial grade of hydrogen gas was fed into the source section and was pumped out by means of a liquid-nitrogen-trapped diffusion pump. The flow rate of the gas was varied by means of a variable leak; the gas pressure within the source section was measured by means of a McLeod gage, and the pressure in the test section was measured by means of an ionization gage.

The magnetic field produced on the geometrical axis of the system by the dc coils is shown in figure 1(b). This field was used to contain the plasma and guide it along the axis of the system.
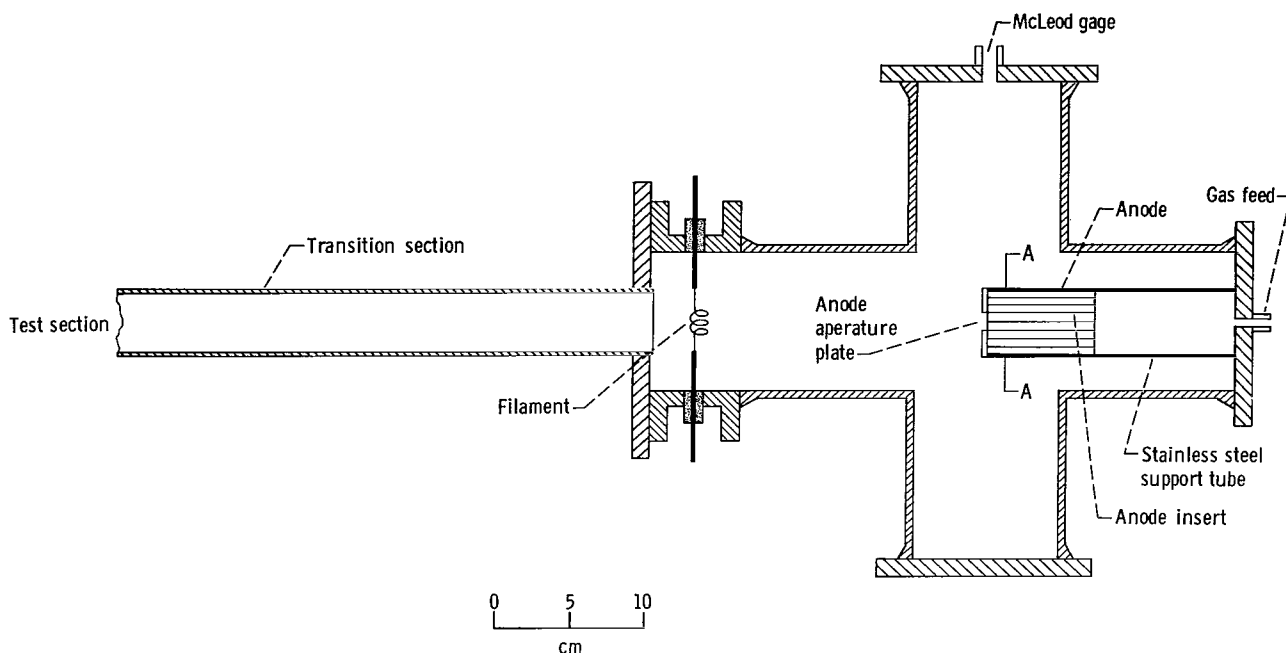
The power supplies for the source consisted of a 0- to 150-volt, 0- to 7.5-ampere beam supply and a 0- to 25-volt, 0- to 25-ampere filament supply. A 5-ohm ballast resistor was placed in series with the beam supply to insure stable operation of the source.

Plasma Source

The basic features of the source are depicted in figure 2. The source consists of a filament, a hollow anode, and an electrically isolated transition section.

The filament consisted of a spiral made from 0.0508-centimeter-diameter tungsten wire and was mounted on insulated feed-throughs.

The hollow anode was made from a 5-centimeter-diameter, 17.8-centimeter-long stainless steel support tube with an anode insert and a tantalum aperture plate. This aperture was 1.9 centimeters in diameter. The anode insert (designed by H. J. Hettel

(a) General features of source.

CD-9613

3.81-cm diam.

0.0508-cm-thick outer shell (molybdenum)

Inner corregated structure made from 0.00762-cm tungsten sheet
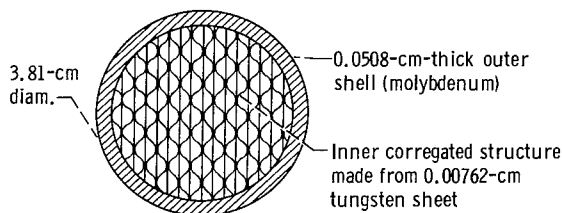
(b) Cross section of anode insert. (Section A-A of fig. 2(a)).

Figure 2. - Representation of hollow anode source.

of Lewis Research Center) was 3.81 centimeters in diameter and 7.62 centimeters long and consisted of a series of channels through which the working gas could be passed. Details of fabrication are given in figure 2(b).

In operation, hydrogen gas is admitted into the source through the anode and is pumped out through the transition section. An electric field is applied between the filament and the anode, and electrons from the filament are accelerated towards the anode.

The anode insert serves two purposes. Since it consists of a series of narrow channels, the gas pressure is higher within this region than within the remainder of the system. Electrons from the filament are guided into this higher pressure region by the magnetic field and can readily ionize the gas which is present. Furthermore, any electrons which strike the walls of the anode insert tend to heat it, thereby causing thermal dissociation of the hydrogen molecule (ref. 4).

The resulting ions are then accelerated in the direction of the filament by the electric fields present between the filament and anode, and pass into the test chamber by way of the transition section. Sufficient electrons are pulled along to insure beam neutrality.

DIAGNOSTIC METHODS AND EQUIPMENT

Radial Distribution of Light Emitters

The distribution of emitters within the plasma is obtained by an examination of the light emitted from it. The variation of emission with plasma operating conditions permits an estimate of the extent of thermal dissociation present.

The plasma is considered optically thin and axisymmetric and is viewed through a pair of collimating slits as shown in figure 3. If the collimating slits are moved paral-

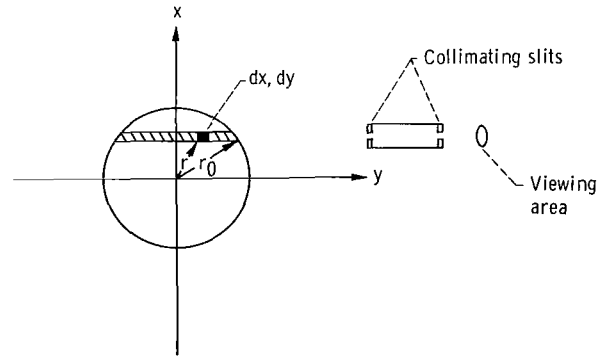Figure 3. - Cross section of plasma considered (z-axis normal to paper).

lel to the x-axis, then a curve of intensity against x may be obtained. If the radiation from each emitter is assumed to be isotropic, then the radial distribution of emitters is given by Abel's transform (ref. 5) as

$$\epsilon(r) = -\frac{1}{\pi} \int_{r}^{r_0} \frac{\frac{dI(x)}{dx}}{\left(x^2 - r^2\right)^{1/2}} \, dx \tag{1}$$

5

where I(x) is the observed intensity distribution and $\epsilon(r)$ is the distribution of emitters. (Symbols are defined in the appendix.)

The emitted radiation was observed by means of a photomultiplier tube which was attached to a pair of collimating slits. Filters were installed between the photomultiplier and the slits. These filters permitted observation of the atomic line at 6562 Å $(6.562 \times 10^{-5}$ cm) or the intense molecular lines at 4062.49 and 4069.65 Å $(4.06249 \times 10^{-5}$ and 4.06965×10^{-5} cm).

Electron Temperature and Plasma Potential

The current-voltage characteristics of a cylindrical Langmuir probe (ref. 6) were analyzed in the following manner to obtain plasma potential. The logarithm of the electron current was plotted as a function of applied probe voltage as shown in figure 4(a). A graph of this type is generally characterized by a region where the current changes exponentially with voltage, followed by a region where a change of probe voltage gives rise to only a small change in current. The intersection of straight lines drawn through these two regions was taken as plasma potential. The current at this point was taken to be the electron saturation current.

The electron temperature can be obtained from the current-voltage characteristic by using the relation

$$\frac{d \ln I_e}{dV} = - \frac{q}{kT_e} \tag{2}$$

where I_e is the electron current and T_e is the electron temperature.

It has been shown (ref. 6) that equation (2) is mathematically equivalent to the expression

$$kT_e = \frac{q(V_p - V_f)}{\ln\left(\dfrac{I_{se}}{I_{si}}\right)} \tag{3}$$

where I_{se} and I_{si} are the saturation electron and ion currents, V_p is plasma potential, and V_f is probe floating potential. (Eq. (3) may be obtained from eq. (2) by integrating and applying the proper boundary conditions.)

Although equations (2) and (3) were shown to be equivalent for the case of a Maxwellian electron energy distribution, they do differ experimentally since different quantities are measured. In most cases either equation (2) or (3) will give the same answer, but there is at least one important case where results may be expected to differ. This

6

(a) Typical probe data for single temperature plasma. If $I_2 = 2.72\ I_1$, then electron temperature $= V_2 - V_1 = 7.8$ eV.

(b) Probe data indicating existence of electrons of two energy groups. [Pressure, 1.68 microns of mercury (0.222 N/m^2); beam current, 7 amperes.]
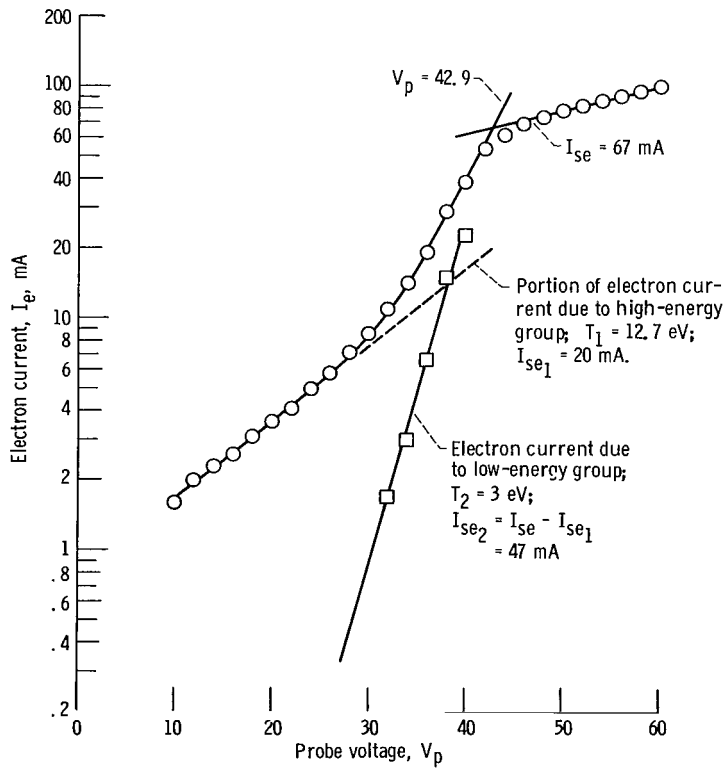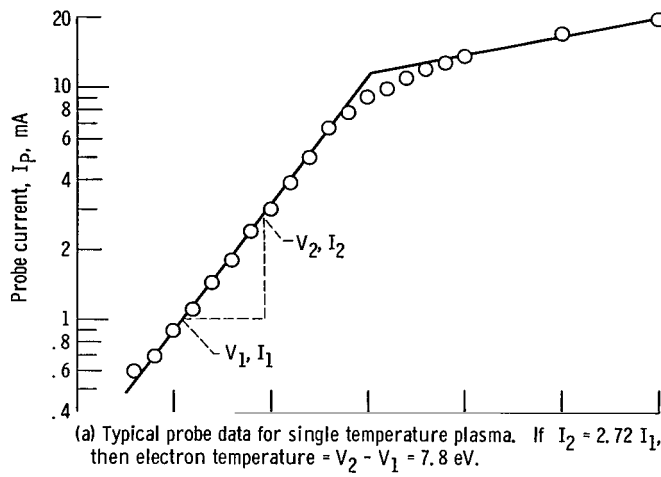
Figure 4. - Experimental probe current-voltage characteristics.

is the case where the electrons are divided into two groups characterized by temperatures T_1 and T_2. The presence of two energy groups gives rise to the probe characteristic shown in figure 4(b). The higher energy portion of the characteristic is given by the linear portion of the experimental data which occurs between 10 and 25 volts. This distribution is depicted by the dashed straight line in the figure. The remaining distribution is obtained by subtracting the dashed straight line from the experimental data. For this case equation (3) will predict a temperature that is somewhere between T_1 and T_2.

Both equations (2) and (3) were used to calculate temperatures in this report and the results are presented in the section RESULTS AND DISCUSSION.

Charged Particle Density

In the absence of a magnetic field, the electron density may be calculated from the electron saturation current and is given by

$$n_I = \frac{I_{se}}{qA_p}\left(\frac{2\pi m}{kT_e}\right)^{1/2} = \frac{3.74 \times 10^{11}}{A_p(kT_e)^{1/2}} \tag{4}$$

where n_I is the electron density in centimeter^{-3}, I_{se} is the electron saturation current in amperes, A_p is the probe area in square centimeters, and kT_e is the electron temperature expressed in electron volts.

Further details about equation (4) and subsequent equations used are given in references 6 to 8.

In the presence of a magnetic field, the assumptions underlying equation (4) break down, and an expression derived by Bohm may be used. This is

$$n_B = \frac{I_{si}M^{1/2}}{0.4\,A_p q(2kT_e)^{1/2}} = \frac{1.13 \times 10^{13}\,I_{si}A^{1/2}}{A_p(kT_e)^{1/2}} \tag{5}$$

where A is the atomic weight of the ion and I_{si} is the saturation ion current in amperes.

A third expression, derived from kinetic theory, may also be used, that is,

$$n_K = \frac{\pi I_{se}(\pi m)^{1/2}}{q A_p (2kT_e)^{1/2}} = \frac{5.87 \times 10^{11} \, I_{se}}{A_p (kT_e)^{1/2}} \tag{6}$$

This equation was derived for the case of a cylindrical probe in a magnetic field and is identical with equation (4) except that the collection area of the probe has been reduced by $2/\pi$. Both equations (5) and (6) were used to obtain density, and it was found that the results lie close to each other in spite of the differences in the basic assumptions.

THEORY FOR VARIATION OF INTENSITY OF BALMER α LINE WITH OPERATING CONDITIONS

The intensity of emission of the 6562 Å (6.562×10^{-5} cm) line from a unit volume of plasma will at any instant be proportional to the density of atoms in their third energy level. In a steady state, the rate of spontaneous emission must be balanced by processes repopulating this level. Therefore, the intensity to be expected will depend directly on the type of process supplying atoms to the third excited state. The discussions that follow are not intended to be rigorous formulations, but are intended to show only the variation of intensity with plasma parameters.

Electron Bombardment

As an approximation to reality, the following assumptions are made:

(1) The atoms are excited directly from the ground state by electrons.

(2) The energy distribution of the electrons is given by a two-temperature Maxwellian of the form

$$f(\epsilon)d\epsilon = n_e \left[x_n A_1 e^{-\epsilon/kT_1} \epsilon^{1/2} \, d\epsilon + (1 - x_n) A_2 e^{-\epsilon/kT_2} \epsilon^{1/2} \, d\epsilon \right] \tag{7}$$

where

$$A_j = \frac{2}{\pi^{1/2}(kT_j)^{1/2}} \tag{8}$$

and x_n is the fractional number of electrons in the first energy group.

9

(3) The excited atoms radiate before they have had time to move from where they were formed.

The rate at which excited atoms are supplied to the third level can be written

$$\frac{dn^*}{dt} = n_H n_e \left[x_n A_1 \int_0^\infty e^{-\epsilon/kT_1} \epsilon \sigma_{13} \, d\epsilon + (1 - x_n) A_2 \int_0^\infty e^{-\epsilon/kT_2} \epsilon \sigma_{13} \, d\epsilon \right]$$

(9)

where σ_{13} is the cross section for exciting a ground state atom to its third energy level.

If the atoms are supplied by thermal dissociation, their number density can be assumed to hold a constant ratio to the original neutral number density n_0. If, on the other hand, the dissociation itself results from electron bombardment, a very approximate assumption can be made that the atom density will be proportional to the product $n_e n_0$. Thus, the intensity to be expected will be

$$\mathscr{I}_{b1} \propto n_0 n_e \left[x_n A_1 \int_0^\infty e^{-\epsilon/kT_1} \epsilon \sigma_{13} \, d\epsilon + (1 - x_n) A_2 \int_0^\infty e^{-\epsilon/kT_2} \epsilon \sigma_{13} \, d\epsilon \right]$$

(10)

or

$$\mathscr{I}_{b2} \propto n_0 n_e^2 \left[x_n A_1 \int_0^\infty e^{-\epsilon/kT_1} \epsilon \sigma_{13} \, d\epsilon + (1 - x_n) A_2 \int_0^\infty e^{-\epsilon/kT_2} \epsilon \sigma_{13} \, d\epsilon \right]$$

(11)

depending on the source of dissociation.

Recombination

If the excited states arise from recombination, a calculation can be based on the following assumptions:

(1) The excited atoms arise from a two-body radiative recombination of electrons

with protons. (Three-body recombination is negligible at the temperatures and pressures considered.)

(2) The energy distribution of the electrons is that given by equation (7).

(3) The rate of production of the third excited state is directly proportional to the total recombination rate.

The total rate can be written

$$\frac{dn_H}{dt} = \sqrt{\frac{2}{m}} \, n_e n_i \int_0^\infty \sigma_r f(\epsilon) \epsilon^{1/2} \, d\epsilon \tag{12}$$

and, from reference 9,

$$\sigma_r \propto \frac{1}{\epsilon} \tag{13}$$

Hence, the expected line intensity would be

$$\mathscr{J}_r \propto n_e^2 \left[\frac{x_n}{(kT_1)^{1/2}} + \frac{(1 - x_n)}{(kT_2)^{1/2}} \right] \tag{14}$$

The three predictions, equations (10), (11), and (14), can be compared with observations as operating conditions are changed. Since the dependence on neutral and electron density differs from model to model, the predictions will differ and the model most closely matching the observations can be determined.

RESULTS AND DISCUSSION

General

As was previously mentioned, the present source could be operated in the following three modes: end chamber grounded, end chamber floating, and end chamber attached to the anode.

Operation in the end-chamber-grounded mode consisted of grounding the end chamber through an ammeter. Both the source current-voltage characteristics and the end chamber current were measured with an x, y-recorder.

In the end-chamber-floating mode, the end chamber was disconnected from the rest of the apparatus and connected to the input of an x, y-recorder. Since the input imped-

ance of the recorder was quite high, the net current to the end chamber was virtually zero.

The third configuration consisted in attaching the end chamber to the anode and measuring the current to the end chamber.

A summary of the range of parameters over which the source was operated is as follows: magnetic field, 0.01 tesla; filament current, 24 amperes; filament power, 260 watts; discharge current, 0 to 8 amperes; discharge voltage, 22 to 108 volts; source-operating pressure, 0.52 to 3.5 microns of mercury (0.069 to 0.475 N/m^2); test chamber pressure, 0.002 to 0.0194 micron of mercury (0.000266 to 0.00258 N/m^2). The neutral pressure within the test chamber (measured with an ionization gage) is given as a function of the pressure within the source chamber in figure 5. This latter pressure was measured with a McLeod gage; both pressures were measured in the absence of a discharge.
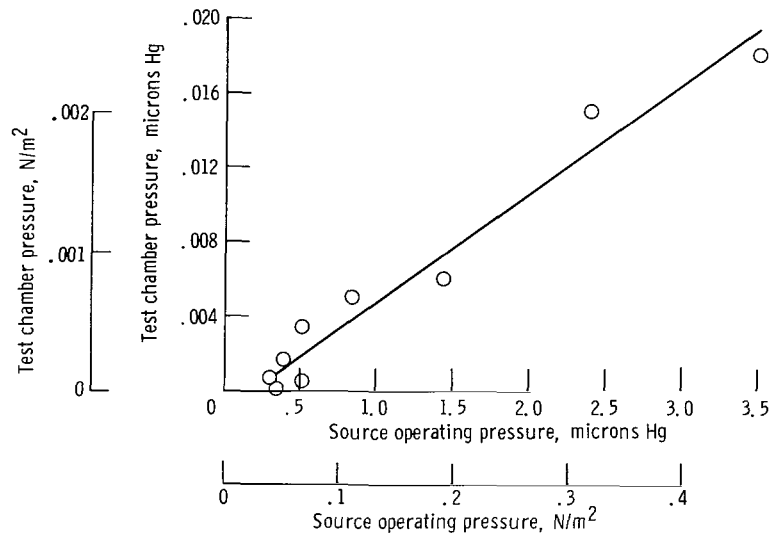

Figure 5. - Background pressure in test chamber as function of source operating pressure. No discharge present.

Most data presented are those which were taken in the end-chamber grounded configuration. Data taken in the other configurations will be presented only insofar as needed to show similarities or differences. The discussion will present data taken within the source section, the test section, and the transition section.

Source Measurements

The only measurements taken within the source section itself were operating pressure and current-voltage characteristics. These current-voltage characteristics are given in figure 6 for the end-grounded configuration. As the pressure is increased, the voltage required to sustain the discharge decreases and becomes more independent of operating current. This is a characteristic feature of a hot cathode discharge.
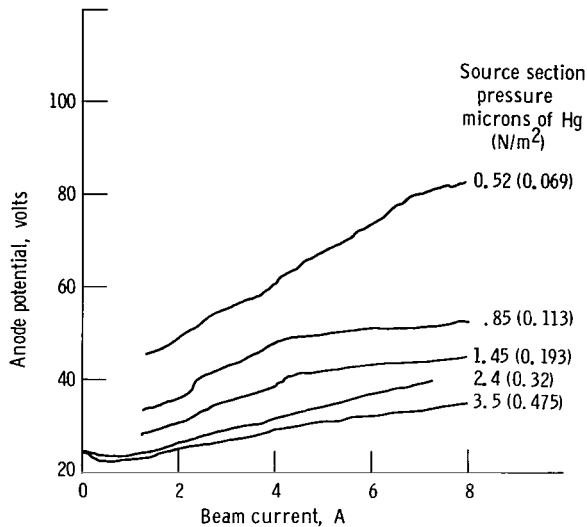

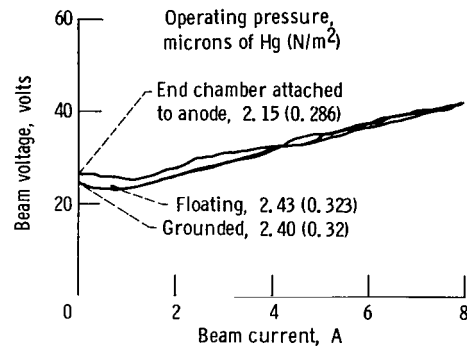Figure 6. – Current voltage characteristics of source with end chamber grounded.

Figure 7. – Current-voltage characteristics of source showing effect of end chamber configuration.

The other two configurations had similar current-voltage characteristics. This is demonstrated in figure 7, where data taken at comparable pressures are presented for the three configurations tested.

The fact that the characteristics were similar for all three configurations implies that the source operates as a true plasma generator in that its operation is independent of the potential of the test section.

Measurements Within the Test Section

The data taken within the test section consisted of probe measurements made on the plasma axis and either the plasma currents to the metal portion of the test chamber (end-grounded and end-attached-to-anode configuration) or its floating potential (end-floating configuration).

13

Plasma potential, electron temperature, and electron density were measured by using a cylindrical probe of 7.9×10^{-7}-square-meter area placed at position A as indicated by the arrow in figure 1(a). These measurements were made along the axis of the plasma. To aline the probe with the plasma axis, the plasma was turned on and a preliminary alinement of the probe was done visually. The floating potential of the probe was then measured for a region about this initial probe position. The probe was then biased negatively with respect to floating potential and was positioned to collect maximum ion current. This point was taken to be the plasma axis.

During the course of the probe alinement, an attempt was made to increase the plasma density within the test chamber by replacing the glass transition piece with a grounded metal section. The grounded metal transition piece destroyed the ability of the source to inject plasma into the test chamber. It is believed that the effect of this transition piece was to alter the plasma potential within this region, thereby either reflecting the ions or driving them into the wall.

The plasma potential (fig. 8) remains relatively constant with beam current at low pressure but shows a marked increase in its current dependence as the pressure is increased. A comparison of figures 6 and 8 indicates that the plasma is at all times close to anode potential, thus providing a mechanism for driving electrons into the test chamber.

Plasma potentials for the other two configurations were nearly the same as those shown in figure 8.

Electron temperatures (figs. 9(a) and (b)) were calculated by using both equations (2) and (3). At the higher beam currents, a group of lower energy electrons (T_2) appeared. Of course, the method using equation (3) can give only a single temperature; this may be considered an effective temperature in the presence of two energy groups. This effective temperature always fell between the two other temperatures obtained. In general, the larger of the two temperatures increased with beam current, which would be the case if it were a function of anode voltage; the lower temperature did not vary greatly. At a given current (7A) the electron temperature decreased with an increase in pressure. The anode voltage exhibited the same characteristics (fig. 6); thus, a direct dependence of electron temperature on anode potential may be inferred.

Operation of the source in the other two configurations did not affect the electron temperature to any significant extent.

The density of charged particles within the system was calculated by using equations (5) and (6). Equation (6) was used with the two temperatures T_1 and T_2 to calculate the fraction of charged particles belonging to each energy group. The means of separating the two saturation electron currents has been indicated in figure 4(b). This fraction was then used in equation (5) with the factor $1/(kT)^{1/2}$ replaced by
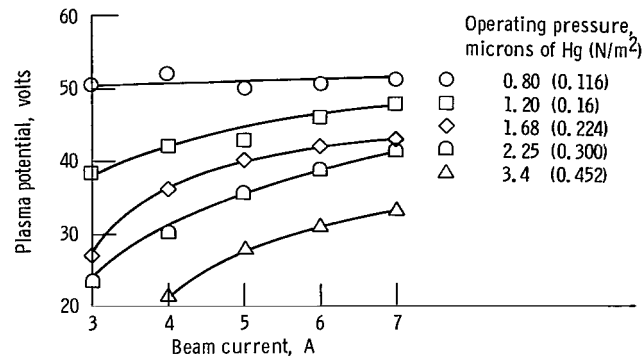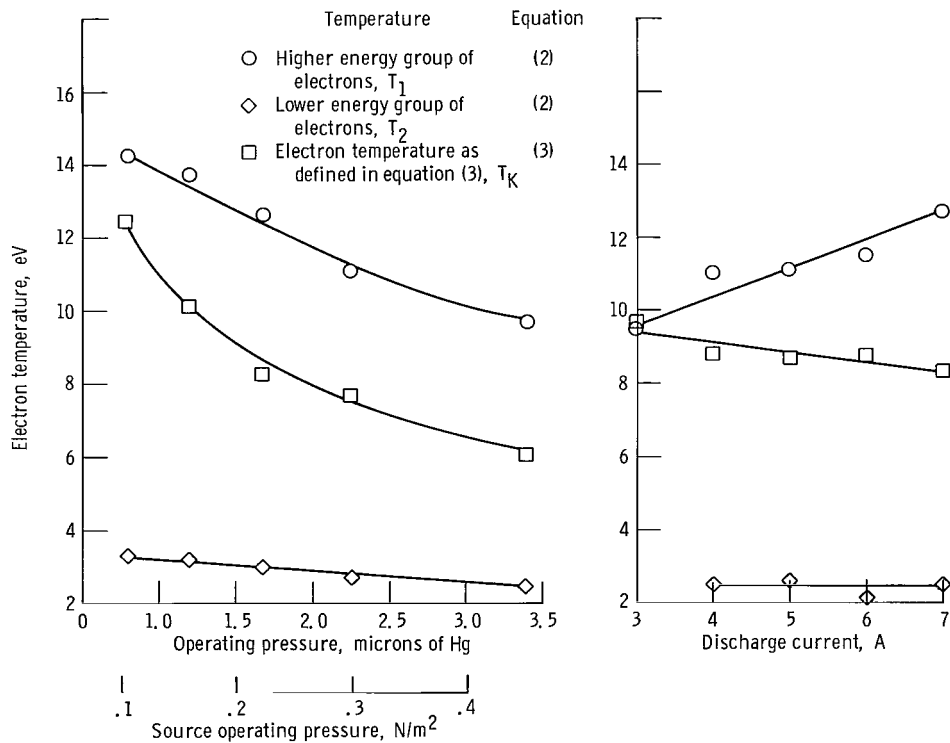
Figure 8. – Potential of plasma in test chamber with end
chamber grounded. Potential measured with respect
to ground.

(a) Effect of operating pressure. Beam current,
    7 amperes.

(b) Effect of discharge current. Operating
    pressure, 1.68 microns of mercury
    $(0.224\ N/m^2)$.

Figure 9. – Electron temperatures on beam axis. End chamber grounded.

$$\frac{x_n}{(kT_1)^{1/2}} + \frac{1 - x_n}{(kT_2)^{1/2}} \tag{15}$$

where

$$x_n = \frac{n_1}{n_1 + n_2} \tag{16}$$

This procedure was used since there was no a priori knowledge of what value of electron temperature to use in equation (5).

Typical variations of density with pressure and beam current are presented in figure 10 using these methods of calculating the density. The most noticeable thing about

	Electron density	Equation
O	Calculated from eq. (6) using temperature T_1, n_{K1}	(6)
◇	Calculated from eq. (6) using temperature T_2, n_{K2}	(6)
□	Sum calculated from eq. (6) using temperatures, T_1 and T_2, $n_{K1} + n_{K2}$	(6)
▽	Calculated from eq. (5), n_B	(5)

(a) Effect of operating pressure. Beam current, 7 amperes.

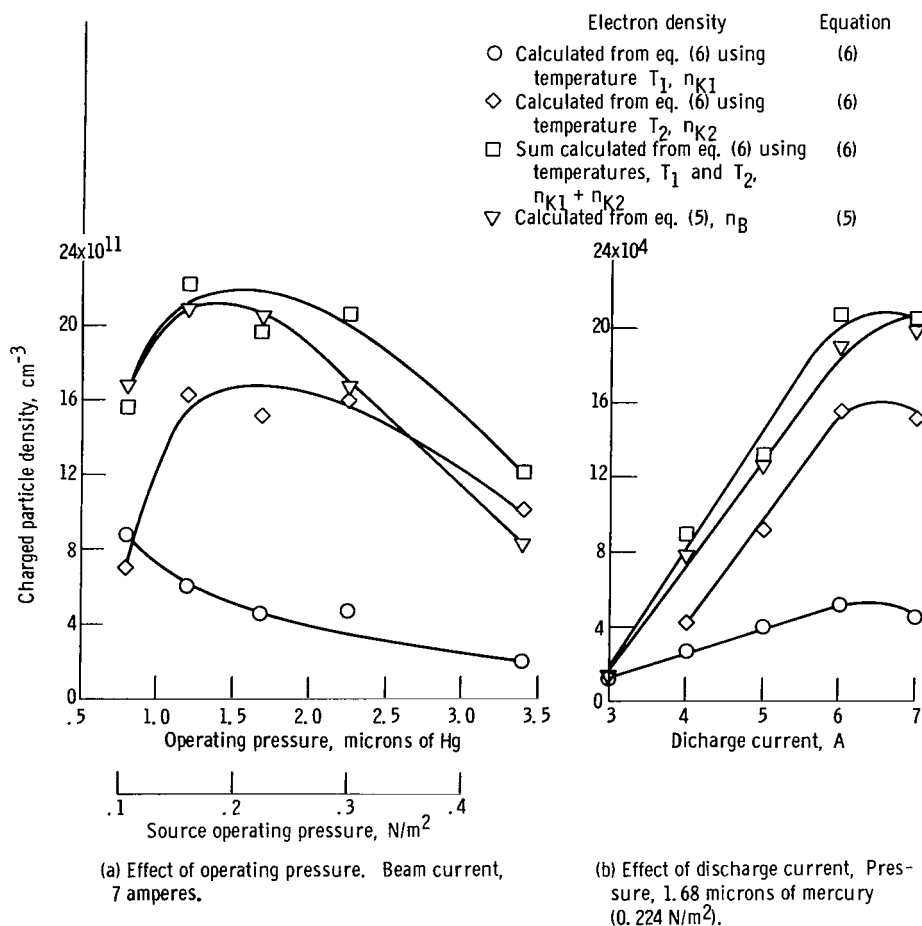(b) Effect of discharge current, Pressure, 1.68 microns of mercury (0.224 N/m²).

Figure 10. - Effect of beam current and operating pressure on charged particle density. End chamber grounded.

the data is that these two methods, even though they make different assumptions about ion temperature, give results which are at worst within 24 percent of each other and are generally much better.

The density increased with current as expected, and it was usually the lower energy electrons that caused most of the increase, both at the higher currents (4 to 7 A) and pressures of 0.85 to 3.4 microns of mercury (0.113 to 0.452 N/m^2). The maximum on-axis density was above 2×10^{12} centimeter^{-3} when the source was operated at a pressure of 1.5 microns of mercury (0.2 N/m^2) and a current of 7 amperes (fig. 10(a)).

Both the total density and the fractional amount of particles in each energy group differed by a small amount when the source was operated in the end-floating or end-attached-to-anode configuration. The densities calculated from equation (6) are presented in figure 11, while the fractional number of particles in the highest energy group is presented in figure 12.
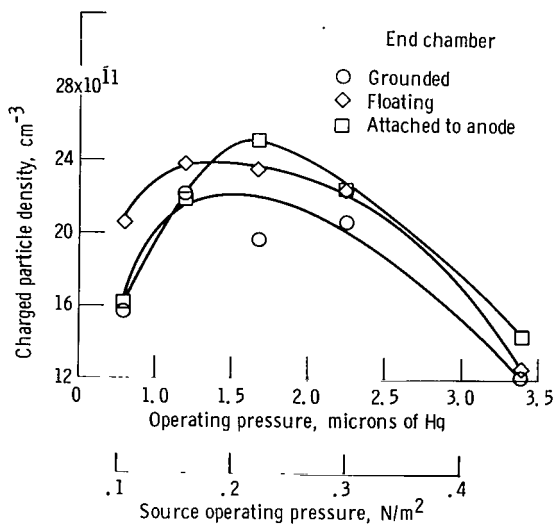

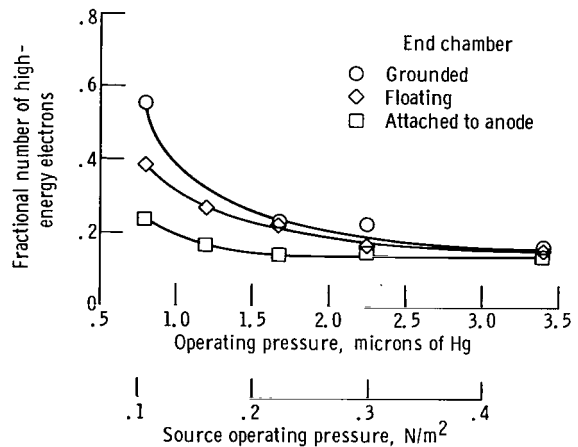Figure 11. – Effect of source configuration on plasma density. Beam current, 7 amperes.

Figure 12. – Effect of source configuration on fractional number of high-energy electrons. Discharge current, 7 amperes.

All three configurations had maximum density near the same pressure of 1.5 microns of mercury (0.2 N/m^2). The end-attached-to-anode configuration gave the highest maximum density of the three tested (fig. 11) but gave the smallest fraction of high-energy particles (fig. 12).

It may be argued that a measurement of electron density at a point just before the plasma enters the metal sleeve does not mean that it is capable of passing through such a sleeve, that is, a grounded sleeve within the test section will short out the beam much like a grounded metal transition section did. To find whether this did indeed happen, the

apparatus was modified (after all data had been taken) to give a uniform magnetic field throughout the test section, and the metal sleeve was separated from the end flange. This separation allowed visual inspection of the plasma striking the end flange. The sleeve and flange were electrically connected and could be left floating, grounded, or attached to the anode. These changes made but slight difference in the appearance of the plasma striking the end flange.

A far more interesting measurement than that of electron density is that of percent ionization, since it was the purpose of this investigation to develop a source of highly ionized plasma. The calculation was made assuming a background density of neutrals obtained from figure 5 along with the electron densities presented. The percent ionization for all three configurations (fig. 13) varied from 65 to 93 percent and decreased
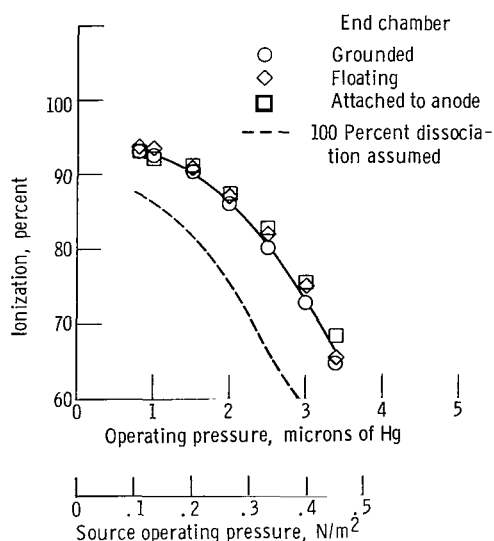

Figure 13. - Percentage of ionization along axis of plasma. Discharge current, 7 amperes.

with an increase in operating pressure. (The percent ionization was defined to be proportional to the charged particle density divided by the sum of the no-plasma neutral density and the charged particle density.)

However, at a high degree of dissociation, the degree of ionization as just defined can be misleading. For example, the background pressure within the test chamber could conceivably increase by a factor of 2 because of dissociation of the hydrogen molecule when the discharge is operating. The percentage ionization calculated assuming complete dissociation is presented as the broken curve in figure 13. The true percentage of ionization is somewhere between the two curves presented.

18

Measurements Within Transition Section

The final series of measurements to be described is the variations of light intensity with operating conditions and the radial profiles of emitter density. The variation of peak emitter density with pressure and beam current is presented in figure 14. These densities were calculated from the atomic line at 6562 Å (6.562×10^{-5} cm). No molecular radiation was observed at 4062.49 Å (4.06249×10^{-5} cm) or at 4069.65 Å (4.06965×10^{-5} cm). The photomultiplier system used was such that the molecular lines
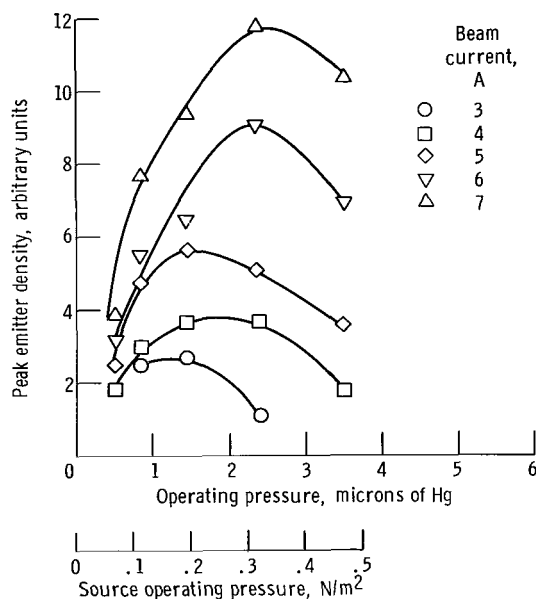

Figure 14. – Variation of peak emitter density (of atomic line at 6562 Å 6.562×10^{-5} cm) with beam current and operating pressure. End chamber grounded.

must have been at least 200 times less intense than the atomic, otherwise they would have been detected. The peak emitter density increases with beam current and, at the higher beam currents, the maximum radiation occurred at a pressure of 2.4 microns of mercury (0.32 N/m^2).

Typical emitter profiles are presented in figure 15(a) for a pressure of 2.4 microns of mercury (0.32 N/m^2) and for several beam currents, and in figure 15(b) for a beam current of 7 amperes at several operating pressures. The variation of plasma radius (defined as the radius at the point where the emitter density has dropped to one-half of its maximum value) with operating pressure and discharge current is given in figure 16.
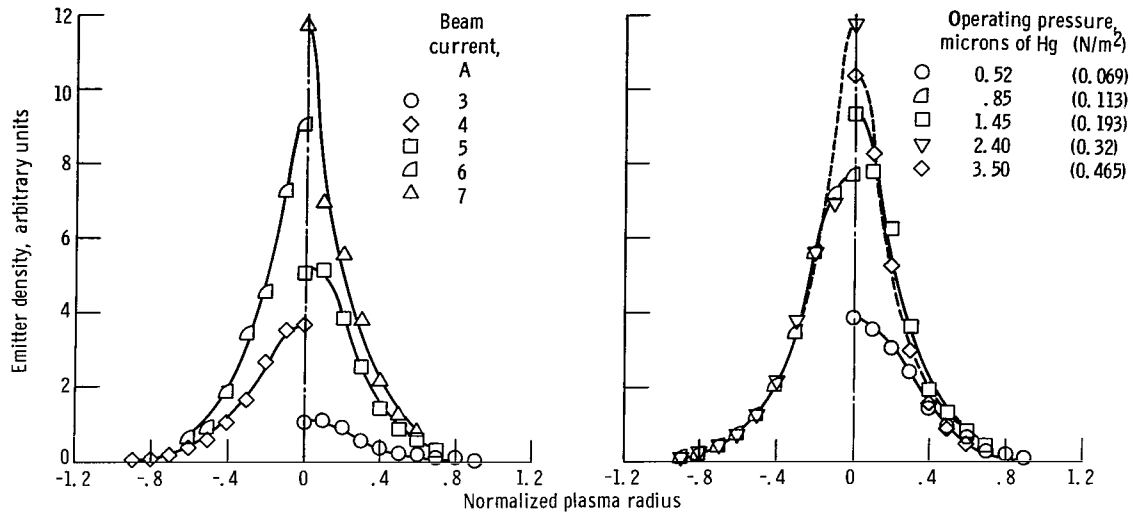
(a) Effect of beam current on emitter profile. Operating pressure, 2.40 microns of mercury (0.32 N/m²).

(b) Effect of operating pressure on emitter profile. Beam current, 7 amperes.

Figure 15. - Typical emitter profiles for end-grounded configuration.

(a) Beam current, 7 amperes.

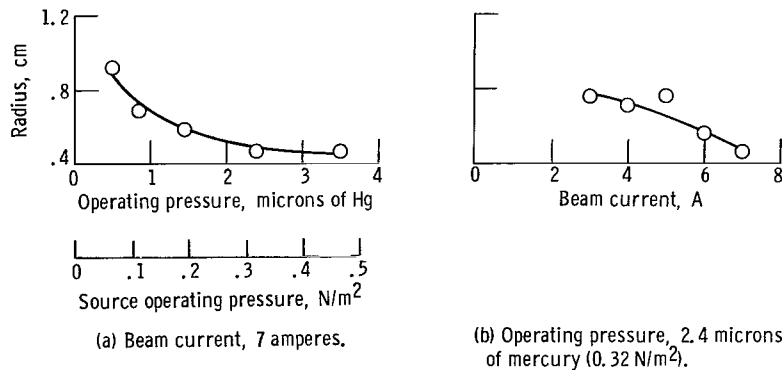(b) Operating pressure, 2.4 microns of mercury (0.32 N/m²).

Figure 16. - Variation of plasma radius with beam current and operating pressure. End chamber grounded.

Generally, the plasma radius decreased as either pressure or beam current was increased.

Operation of the source in the end-float or end-to-anode configuration did not materially affect the results of the light intensity measurements.

Experimental values of n_0, n_e, T_1, T_2, and x_n were inserted into the theoretical expressions (eqs. (10), (11), and (14)), and the results are presented in figure 17. The results were normalized to agree at the initial beam current of 3 amperes.

The model that assumed thermal dissociation (eq. (10)) came closest to the experimental data. This supports the view that thermal dissociation plays a dominant role in the formation of atoms within this source.
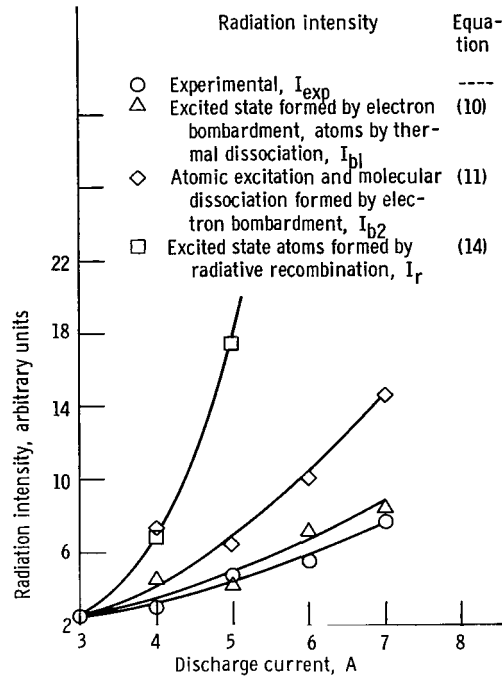
Radiation intensity   Equation

○   Experimental, I_{exp} ----
△   Excited state formed by electron   (10)
    bombardment, atoms by ther-
    mal dissociation, I_{b1}
◇   Atomic excitation and molecular   (11)
    dissociation formed by elec-
    tron bombardment, I_{b2}
□   Excited state atoms formed by   (14)
    radiative recombination, I_r

Radiation intensity, arbitrary units

Discharge current, A

Figure 17. – Comparison of theoertical pre-
dictions of variation of light intensity with
experiment. Operating pressure, 0.8 micron
of mercury (0.106 N/m^2).

CONCLUDING REMARKS

A source designed to produce a highly ionized plasma of moderate density was tested to determine its operating characteristics. The source consisted of a hot cathode discharge with the following unconventional features: (1) the anode was gas fed and designed to thermally dissociate the hydrogen molecule, and (2) the plasma which was formed was allowed to diffuse from the anode-cathode interspace, past the cathode, and into the test chamber through a glass transition section.

The current-voltage characteristics of the source depended only on pressure. The location of the metal portion of the test chamber in the electrical circuit was unimportant.

The plasma potential remained close to the anode potential and was unaffected by the connection of the test chamber.

The electrons were divided into two groups of differing temperatures. In general, the temperature of the higher energy group was about three times that of the lower. The temperature of the higher energy group varied from 9.5 to 14.3 electron volts, while that of the low-energy group varied from 2.1 to 3.3 electron volts. Both temperatures decreased with an increase in pressure when the beam current was held constant. The

density of particles in the low-energy group did not vary with beam current when the pressure was held constant. The electron temperatures were unaffected by the test chamber connection.

The maximum ion density occurred at a pressure near 1.5 microns and a discharge current of 7 amperes. It exceeded 2×10^{12} centimeter^{-3} when the test chamber was grounded. The density differed when the test chamber was allowed to float, or was connected to the anode. The percentage ionization varied from 65 to 93 percent as the pressure was varied and the discharge current was held at 7 amperes.

Measurements of emitter profile and relative values of peak emitter density were obtained by observing the light emitted from the transition section. In general, the radius of the plasma decreased with an increase in both pressure and discharge current. The emitter measurements were unaffected by the test chamber connection.

The variation in peak emitter density with discharge current was observed. This variation was consistent with that calculated assuming thermal dissociation within the anode and excitation by electron bombardment.

Lewis Research Center,
    National Aeronautics and Space Administration,
        Cleveland, Ohio, March 18, 1968,
            129-01-05-09-22.

APPENDIX - SYMBOLS

A atomic weight of ion

A_p probe area

A_1 normalizing factor

A_2 normalizing factor

$f(\epsilon)d\epsilon$ electron energy distribution function

I current

I_e electron current

I_{se} saturation electron current

I_{si} saturation ion current

I_x light intensity at point x

$\mathscr{J}$ intensity of radiation of 6562 Å atomic hydrogen line

$\mathscr{J}_{b1}$ intensity of radiation when excited state is formed by electron bombardment and atoms are formed by thermal dissociation

$\mathscr{J}_{b2}$ intensity of radiation when atomic excitation and molecular dissociation are formed by electron bombardment

$\mathscr{J}_r$ intensity of radiation when excited state atoms are formed by radiative recombination

k Boltzmann constant

M ion mass

m electron mass

n_B electron density calculated from eq. (5)

n_e electron density

n_H proton density

n_I electron density calculated from eq. (4)

n_K electron density calculated from eq. (6)

n_0 neutral particle density

n_1 density of electrons of temperature T_1

n_2 density of electrons of temperature T_2

n^* density of excited states

q electronic charge

r radius

T_e electron temperature

T_K electron temperature as defined in eq. (3)

T_1 temperature of higher energy group of electrons

T_2 temperature of lower energy group of electrons

t time

V voltage

V_f probe floating potential

V_p plasma potential

x_n fractional composition, eq. (20)

ϵ electron energy

$\epsilon(R)$ emitter density at radius r

σ_r cross section for electron-ion recombination

σ_{13} cross section for exciting ground state atom to its third energy level

τ average lifetime of excited state atom

24

REFERENCES

1. Swett, Clyde C.; and Krawec, Roman: Experiments on Ion-Cyclotron Wave Generation, Using an Electrostatically Shielded RF Coil. Bull. Am. Phys. Soc., vol. 10, no. 4, 1965, p. 509.

2. Swett, Clyde C.: Effect of Magnetic Beach on RF Power Absorption in Ion Cyclotron Resonance. Bull. Am. Phys. Soc., vol. 11, no. 4, 1966, p. 450.

3. Krawec, Roman; Prok, George M.; and Swett, Clyde C.: Evaluation of Two Direct-Current Methods of Plasma Production for Use in Magnetic Mirror Experiments. NASA TN D-2862, 1965.

4. Hickmott, T. W.: Interaction of Hydrogen with Tungsten. J. Chem. Phys., vol. 32, no. 3, Mar. 1960, pp. 810-823.

5. Bockasten, K.: Transformation of Observed Radiances into Radial Distribution of Emission of Plasma. J. Opt. Soc. Am., vol. 51, no. 9, Sept. 1961, pp. 943-947.

6. Glasstone, S.; and Lovberg, R. H.: Controlled Thermonuclear Reactions; an Introduction to Theory and Experiment. D. Van Nostrand Co., Inc., 1960.

7. Krawec, Roman: Radial Density and Temperature Profiles at the Ion Cyclotron Wave Resonance Point. AIAA J., vol. 4, no. 12, Dec. 1966, pp. 2166-2170.

8. Huddlestone, Richard H.; and Leonard, Stanley L.: Plasma Diagnostic Techniques. Academic Press, 1965.

9. Dewan, Edmond M.: Generalizations of the Saha Equation. Phys. Fluids, vol. 4, no. 6, June 1961, pp. 759-764.

"The aeronautical and space activities of the United States shall be conducted so as to contribute . . . to the expansion of human knowledge of phenomena in the atmosphere and space. The Administration shall provide for the widest practicable and appropriate dissemination of information concerning its activities and the results thereof."

— NATIONAL AERONAUTICS AND SPACE ACT OF 1958

NASA SCIENTIFIC AND TECHNICAL PUBLICATIONS

TECHNICAL REPORTS: Scientific and technical information considered important, complete, and a lasting contribution to existing knowledge.

TECHNICAL NOTES: Information less broad in scope but nevertheless of importance as a contribution to existing knowledge.

TECHNICAL MEMORANDUMS: Information receiving limited distribution because of preliminary data, security classification, or other reasons.

CONTRACTOR REPORTS: Scientific and technical information generated under a NASA contract or grant and considered an important contribution to existing knowledge.

TECHNICAL TRANSLATIONS: Information published in a foreign language considered to merit NASA distribution in English.

SPECIAL PUBLICATIONS: Information derived from or of value to NASA activities. Publications include conference proceedings, monographs, data compilations, handbooks, sourcebooks, and special bibliographies.

TECHNOLOGY UTILIZATION PUBLICATIONS: Information on technology used by NASA that may be of particular interest in commercial and other non-aerospace applications. Publications include Tech Briefs, Technology Utilization Reports and Notes, and Technology Surveys.

Details on the availability of these publications may be obtained from:

SCIENTIFIC AND TECHNICAL INFORMATION DIVISION

NATIONAL AERONAUTICS AND SPACE ADMINISTRATION

Washington, D.C. 20546